International Journal of Greenhouse Gas Control 19 (2013) 251–261

Contents lists available at ScienceDirect

International Journal of Greenhouse Gas Control

journal homepage: www.elsevier.com/locate/ijggc

# Optimal design of pressure-based, leakage detection monitoring networks for geologic carbon sequestration repositories

Alexander Y. Sun*, Jean-Philippe Nicot, Xiaodong Zhang

*Bureau of Economic Geology, Jackson School of Geosciences, The University of Texas at Austin, Austin, TX 78758, United States*

ARTICLE INFO

*Article history:*
Received 10 June 2013
Received in revised form 9 August 2013
Accepted 6 September 2013
Available online 4 October 2013

*Keywords:*
Geological carbon sequestration
Leakage along wells
Early leakage detection
Optimal monitoring network design
Integer programming

ABSTRACT

Monitoring of leakage at geologic carbon sequestration (GCS) sites requires the capability to intercept and resolve the onset, location, and volume of leakage in a timely manner. Pressure-anomaly monitoring represents one of the few monitoring technologies that possess such capabilities. To fully leverage the strength of pressure monitoring while meeting cost constraints, optimization of network design is necessary. This study presents an optimization method for designing cost-effective GCS monitoring networks under model and parameter uncertainty. A binary integer programming problem (BIPP) is formulated to minimize both the total volume of leakage and the number of uncovered potentially leaky locations. The BIPP is demonstrated for selecting optimal monitoring locations in both homogeneous and heterogeneous formations. The sensitivity of monitoring design to a number of model and design parameters is investigated, while model structure and parameter uncertainties are incorporated through user-specified scenarios. Results suggest that the BIPP is a viable approach for identifying optimal sensing locations even when the number of design variables is relatively large ($\sim 10^5$). The BIPP is general and can be readily used to facilitate the design of performance-based GCS monitoring networks.



## 1. Introduction

Carbon capture and sequestration (CCS) has the potential of enabling deep reduction in global carbon dioxide ($CO_2$) emissions. To fully realize this potential on a level that matters to climate change mitigation, an industrial-scale geologic carbon sequestration (GCS) repository must have the capacity to store large volumes of $CO_2$ from major emission facilities. In 2011, the total capacity of coal-fired generators in the U.S. amounted to 318 GW (U.S. Energy Information Administration, 2012). A one-GW, coal-fired power plant generates on average 5–10 million tons of $CO_2$ annually during a typical 30-year plant life. Injection of large volumes of $CO_2$ may cause large-scale subsurface pressurization over tens or even hundreds of square kilometers, and may adversely affect nearby natural resources if unintended migration of brine or injected fluids occurs (Birkholzer and Zhou, 2009; Pruess, 2004). A major environmental concern is whether underground drinking water sources overlying the GCS repository can be affected in the presence of potential leakage pathways. To protect public health and environmental safety, a comprehensive risk profile must be established for each GCS project.

In the U.S., the risk-informed, performance-based regulatory view has long been adopted by environmental and nuclear regulatory agencies. Future CCS regulations are most likely to be modeled after these existing risk-informed regulatory frameworks (Wilson et al., 2007). Like many environmental problems, leakage caused by $CO_2$ injection can have both legal and financial implications for institutions involved. Regulators must devise an appropriate penalty or incentive scheme such that GCS licensees are motivated to adopt state-of-the-art monitoring technologies, as well as optimal monitoring plans, throughout the lifecycle of a GCS project.

A large number of GCS monitoring, mitigation, and verification (MMV) technologies have recently been developed and field demonstrated, including pressure and temperature monitoring, geophysical surveys, groundwater chemistry monitoring, soil gas isotopic analysis, remote-sensing of surface deformations, and measurement of tracers co-injected with the $CO_2$ stream (e.g., Benson, 2007; Lewicki et al., 2005; Romanak et al., 2012; Rutqvist et al., 2010; Seto and McRae, 2011). For model-based leakage risk assessment, a large number of analytical and numerical models have been developed to quantify the response of overlying aquifers to potential leakage events (e.g., Celia et al., 2011; Cihan et al., 2011; Nordbotten et al., 2005a; Oldenburg and Unger, 2003; Zhou et al., 2008) and their detectability under parameter uncertainty (Buscheck et al., 2012; Oladyshkin et al., 2011; Sun and Nicot, 2012; Sun et al., 2013). Each type of monitoring technology has a certain detection range. Thus, optimization is necessary for maximizing the utility of these monitoring technologies, especially when financial resources are limited and future CCS policies remain uncertain.

* Corresponding author. Tel.: +1 512 475 6190; fax: +1 512 471 0140.
*E-mail address:* alex.sun@beg.utexas.edu (A.Y. Sun).

1750-5836/$ – see front matter © 2013 Elsevier Ltd. All rights reserved.
http://dx.doi.org/10.1016/j.ijggc.2013.09.005

Trabucchi et al. (2010) grouped the costs and financial responsibilities related to GCS into three categories: (a) costs related to site characterization, construction, and operations; (b) costs related to inflation, technology, and policy changes; and (c) damages resulting from unplanned events (e.g., leakage and induced seismicity). While item (a) largely represents fixed costs, items (b) and (c) can be uncertain and have been perceived as a major hurdle to industrial-scale implementation of GCS projects (Wilson et al., 2008). Any performance-based CCS regulatory framework should differentiate between damage caused by negligence and that by accidents in such a way that preventive activities are rewarded. Examples of preventive activities include, but are not limited to, use of innovative and effective monitoring technologies and optimal design of monitoring networks.

Most in situ GCS monitoring networks are location sensitive, especially when the main monitoring goal is focused on early detection. Yang et al. (2011) evaluated detectability of $CO_2$ leakage flux in the near surface environment for different monitoring network densities and parameter ranges. They concluded that surface soil $CO_2$ flux measurement alone is unlikely to be feasible as a standalone technology for leakage detection and it would be most effective if applied in high-risk locations, such as areas near abandoned wells. Dooley et al. (2010) stressed the importance of tailoring the monitoring design to site-specific risk profiles (as opposed to an idealized average site) and imputing expected probable loss values according to these profiles. So far, limited work has been done on optimizing the design of GCS monitoring networks for cost-effective and timely $CO_2$ leakage detection. In this work we demonstrate such a network optimization process for pressure-based leakage monitoring.

Pressure monitoring is one of a few MMV technologies that can reveal not only the presence, but also the *onset*, *location*, and *volume* of leakage with relatively high accuracy and broad coverage (Jung et al., 2013; Sun and Nicot, 2012). Knowledge of these three leakage attributes is likely to constitute a major component of performance-based CCS regulations for assessing consequences of environmental damage. Downhole pressure monitoring in deep above-zone monitoring intervals (AZMI) has been proposed for early detection of leakage (Hovorka et al., 2013) because of the fast traveling speed of pressure perturbations and the proximity of deep AZMI to storage formations (Nordbotten et al., 2004). For example, in the Texas Gulf Coast region in the U.S., which is home to several proposed and operating GCS sites, the deep AZMI is a regional saline aquifer overlying the storage formation (Hovorka et al., 2013). Unlike monitoring directly in the storage formation, AZMI monitoring may be subjected to less pressure disturbance induced by production activities, provided that pressure anomaly signals can be intercepted by the network. Operation wise, deep pressure monitoring wells are costly to drill and maintain—drilling and instrumentation costs can easily exceed $1 million per well, which is in addition to annual maintenance and operation costs (U.S. Environmental Protection Agency, 2010). Thus, there is strong incentive to optimize the design of pressure-based monitoring networks.

The general concept of environmental monitoring network optimization is not new and has been studied elsewhere. Previous studies have focused on groundwater quality compliance (Loaiciga, 1989; Loaiciga et al., 1992; Meyer et al., 1994; Reed and Minsker, 2004), early warning systems for water distribution network contamination (Berry et al., 2006; Krause et al., 2008; Xu et al., 2010), contaminant source identification (Dhar and Datta, 2007; Mahar and Datta, 1997; Sun et al., 2006), and experimental design (Bayer et al., 2010; Singh and Minsker, 2008; Uciński and Patan, 2007). Although our optimization problem is built on elements of those previous studies, the application to pressure-based monitoring network design is new, requiring the tailoring of design objectives for GCS monitoring.

Common objectives of environmental monitoring networks are minimization of total pollutant spills and maximization of coverage (Meyer et al., 1994; Xu et al., 2010). The former requires that sensors be placed as close as possible to sources, while the latter requires that the area of review be covered to the greatest extent possible. In the current context, the sensor placement problem is complicated by uncertain characteristics of leaking sources and uncertainty in the forward simulation model. We follow a scenario-based approach, which assumes that a limited number of leakage scenarios can be identified a priori on the basis of vulnerability assessment. Initially the prior information obtained from site characterization is used to reduce uncertainty in the design model or to prioritize target monitoring areas. A suite of scenarios are then developed to reflect a site operator's preferences and the site's risk profile. Such a scenario-based approach is inherently consistent with established GCS risk-assessment frameworks, which call for the identification of features, events, and processes for each proposed GCS site during risk assessment (Benson, 2007; DOE/NETL, 2011).

The remainder of the paper is organized as follows. In the next section, we describe the formulation and solution of our monitoring network optimization problem. Section 3 demonstrates the design of the optimal monitoring network for both homogeneous and heterogeneous formations. Stratified sedimentary deposits can form multiple permeability modes across scales, corresponding to a hierarchy of sedimentary unit types (Lunt et al., 2004; Sun et al., 2008). Again in the case of Texas Gulf Coast region, lengths of fluvial channels are on the order of 100–1000 m in the AZMI (Nuñez-López et al., 2011; Young et al., 2006). The presence of large-scale features can impose significant challenges on monitoring network design: on the one hand, preferential flow channels may attenuate pressure anomaly signals significantly before they are even detected; on the other hand, spatial distribution and connectivity of buried channels can never be known exactly. We show how prior information (e.g., permeability range or facies distribution) may be synthesized to generate different scenarios and how network configurations can be determined by making tradeoffs between the two objectives. The last section summarizes the main findings. For the rest of this discussion, we shall use the terms *sensor* and *monitoring well* interchangeably.

## 2. Problem formulation

Let us assume that we have identified a priori a set of locations (or areas) $\mathcal{I}$ with high leakage risks. Corresponding to $\mathcal{I}$, we have also identified a set of monitoring sites, $\mathcal{J}$, which can be either centroids of a grid covering the area of review, or custom locations selected according to the site risk profile. This approach implicitly discretizes the infinite decision space into a finite one and has been commonly adopted in sensor network design literature for obtaining heuristically optimal solutions (Krause et al., 2008; Meyer et al., 1994; Zou and Chakrabarty, 2004). For the purpose of this work, a *leakage event* is defined as an event that starts at the onset of leakage until the anomaly signal is first detected by a sensor, or the site-specific maximum detection time, $T_{max}$, is exceeded, whichever happens first. If the leakage event cannot be detected by any sensor during $T_{max}$, it is deemed an undetected event. In either case, the accumulative volume of leakage during the elapsed time interval can be calculated. A *scenario* is a pre-defined setting for capturing a certain aspect of conceptual or parametric uncertainty.

The maximum detection time, $T_{max}$, may have both regulatory and practical significance. First, it responds to the notion of "early detection" and forms a fundamental basis for prioritizing

monitoring locations. Second, it provides a measure of containment and, thus, forms the basis for rulemaking. Thus, it makes sense to either stipulate $T_{max}$ for a site directly, or limit the maximum volume of fluids (brine or $CO_2$) that is allowed to migrate from a storage formation due to leakage. The latter measure, as proposed in Stenhouse et al. (2009), can be used to derive $T_{max}$ indirectly. The main focus of this work is brine leakage, which may deteriorate drinking water quality and typically occurs earlier than $CO_2$ leakage in the lifecycle of GCS projects.

For our monitoring network design problem, the overall goal is to identify a subset of $\mathcal{J}$ that can optimize the objective function across all user-defined scenarios while satisfying design and budget constraints. Mathematically, the sensor placement problem is formulated as a p-median problem:

$$\min \left\{ V + \lambda G \right\} \tag{1}$$

subject to

$$V = \sum_{s \in \mathcal{S}} \sum_{i \in \mathcal{I}} \sum_{j \in \mathcal{J}_d} v_{ijs} x_{ijs}, \tag{2}$$

$$G = \sum_{s \in \mathcal{S}} \sum_{i \in \mathcal{I}} g_{is} \tag{3}$$

$$g_{is} + \sum_{j \in \mathcal{J}_d} x_{ijs} = 1, \quad i = 1, \ldots, I, \forall s \in \mathcal{S} \tag{4}$$

$$N g_{is} + \sum_{j \in \mathcal{J}_d} z_j \leq N, \quad i = 1, \ldots, I, \forall s \in \mathcal{S} \tag{5}$$

$$\sum_{j=1}^{N_m} z_j = N \tag{6}$$

$$z_j \geq x_{ijs}, \quad \forall i \in \mathcal{I}, j \in \mathcal{J}_d, s \in \mathcal{S} \tag{7}$$

$$x_{ijs} \in \{0, 1\}, \quad \forall i \in \mathcal{I}, j \in \mathcal{J}_d, s \in \mathcal{S} \tag{8}$$

$$z_j \in \{0, 1\}, \quad \forall j \in \mathcal{J} \tag{9}$$

$$g_{is} \in \{0, 1\}, \quad i = 1, \ldots, \mathcal{I}, \forall s \in \mathcal{S} \tag{10}$$

The symbols are defined as follows:

$V$ is the total volume of leakage by all leakage events and across all scenarios;
$G$ is the number of undetected leakage events across all scenarios;
$\lambda > 0$ is the relative weight between two objectives $V$ and $G$;
$\mathcal{I}$ is a set of potential leak locations and $N_l$ is the number of elements in $\mathcal{I}$;
$\mathcal{J}$ is a set of candidate sensor locations and $N_m$ is the total number of elements in $\mathcal{J}$;
$\mathcal{J}_d$ is a subset of $\mathcal{J}$ that can respond to a particular leakage event;
$\mathcal{S}$ is a set of user-defined scenarios and $N_s$ represents the number of elements in $\mathcal{S}$;
$v_{ijs}$ is the accumulative volume of leakage at the time of initial detection for a leak event in scenario $s$ that originated from location $i$ and is detected by sensor $j$;
$x_{ijs} = 1$, if a leak event from location $i$ is detected by sensor $j$ in scenario $s$, and 0 otherwise;
$z_j = 1$, if a sensor is placed at location $j$, and 0 otherwise;
$g_{is} = 1$, if a leak event originated from location $i$ is not detected by any sensor in scenario $s$, and 0 otherwise; and $N$ is the number of sensors that can be budgeted.

The sensor placement problem specified by Eqs. (1)–(10) optimizes a weighted sum of two conflicting objectives, namely, minimization of total leakage volume $V$ and maximization of network coverage (or minimizing $G$) across all scenarios. Eq. (2) defines the total amount of leakage, in which the accumulative leakage term, $v_{ijs}$, for each leakage event is defined as

$$v_{ijs} = \int_{t_0}^{t_0+T} q_l(\tau) d\tau, \tag{11}$$

where $q_l$ is leakage rate; $t_0$ is start time of leak; $T$ is either time to the first detection or, in case that all sensors fail to detect the event, the $T_{max}$; and $\tau$ is an integration variable. Eq. (3) counts the number of undetected leakage events for all scenarios. Constraint (4) ensures that each leakage event is either detected by a sensor in $\mathcal{J}$ or undetected during $T_{max}$ (i.e., $g_{is} = 1$). Constraint (5) requires that the monitoring network be able to detect a leakage event when the event is detectable; in other words, the variable $g_{is}$ is set true only when the subset $\mathcal{J}_d$ is empty. Constraint (6) specifies the actual number of monitoring wells that can be deployed, which is determined on the basis of potential risks and costs. Constraint (7) precludes the situation that a leakage event is detected when subset $\mathcal{J}_d$ is empty. Finally, constraints (8)–(10) merely specify that all decision variables, $x_{ijs}$, $z_j$, and $g_{is}$ are binary integer variables. Note that our formulation of the p-median problem is similar to that presented in Meyer et al. (1994) and Xu et al. (2010). However, the former work did not consider scenarios, whereas the latter did not include constraints (4) and (5) that are needed to arrive at optimal solutions in our case.

In this study, we formulate and solve an a priori network design problem, as opposed to a sequential design approach in which monitoring wells are added one at a time as new information becomes available. Our assumption is that the licensee is risk averse and would like to maximize the use of present resources to minimize perceivable future damage. In other words, the expected costs associated with the alternative wait-and-see option would be too high for the licensee to select. Note that we have assumed that all scenarios have equal weights. If not, a weight factor can be assigned to each scenario. Calculation of the constraint in Eq. (2) is the most computationally demanding step, requiring running the forward model for all combinations of leaky and monitoring sites; however, the constraint is independent of the number of sensors and the results can be reused when the only design change is the number of sensors.

Objective function specified in (1) is known as the weighted global criterion method for multiobjective optimization and has been used in many previous studies (Meyer et al., 1994; Xu et al., 2010). A general goal of multiobjective optimization is to identify members of the Pareto optimal set which contains all non-dominated solutions. The weighted global criterion can be considered a utility function for expressing a decision maker's preference by assigning weights to different objectives. If all weights are positive and the global criterion (1) increases monotonically with respect to each objective function, then minimization of criterion (1) yields Pareto optimal solutions (Stadler, 1988). Because the two quantities in criterion (1) have different dimensions, a standard practice in the literature is to normalize each objective such that $\lambda$ is restricted to varying in [0,1]. Such calculation requires knowledge of the bounds of each objective. In practice, the weighted global criterion method is used primarily for incorporating a priori articulation of preference, in which case the user indicates his/her preference before running the optimization algorithm and lets the algorithm determine a single solution that reflects such preferences. A more likely situation during monitoring network design is a posteriori articulation of preference, in which the user first generates a Pareto optimal set and then selects a solution from the set based on tradeoffs between objectives. For the latter purpose, we may convert objective function (1) into a single-objective problem by treating the coverage requirement as a user-specified upper

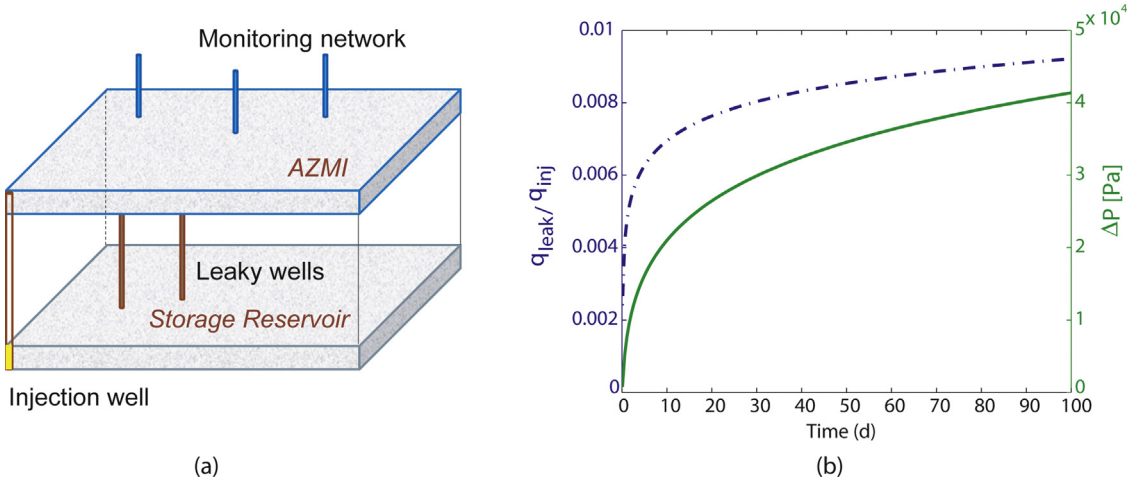


**Fig. 1.** (a) Schematic drawing of problem setup, in which storage formation (lower layer) and AZMI (upper layer) are separated by a confining layer (not to scale). An injection well is screened in the storage formation; and pressure responses are observed in the AZMI; (b) example of leakage rates and pressure anomalies obtained for homogeneous aquifers. Left axis: ratio between leakage rate and injection rate; right axis: pressure anomalies. Note the detection threshold is set to 0.1 bar ($10^4$ Pa) in this study.

bound of uncovered nodes. Thus, objective function (1) is replaced by

$$\min V \tag{1'}$$

and the constraint (3) is replaced by

$$G' = \frac{1}{N_I N_S}\sum_{s\in\mathcal{S}}\sum_{i\in\mathcal{I}} g_{is}, \quad G' \le 1 - B \tag{3'}$$

in which $0 < B \le 1$ is the desired coverage ratio specified by the user, and $G'$ represents the average ratio of uncovered nodes across all scenarios. Remaining constraints are the same as before. By running the single-objective problem for different coverage ratios, we can effectively construct a Pareto front.

The single-objective formulation is adopted here for the aforementioned reasons, leading to a binary integer programming problem (BIPP). Theories for solving BIPPs are well-established and generally include (a) enumeration techniques (e.g., branch-and-bound), (b) cutting-plane techniques, and (c) group-theoretic techniques. For example, the commonly used branch-and-bound algorithm is a heuristic strategy that divides the feasible region into subregions and searches for the feasible solution by solving a series of linear programming relaxation problems, in which the binary variables are replaced by (0, 1) continuous variables (Boyd and Vandenberghe, 2004). In this study, all BIPP problems were solved using the Matlab toolbox, Gurobi, which is a highly efficient optimization solver for both integer and mixed integer programming problems (Gurobi, 2012).

## 3. Results and discussion

### 3.1. Homogeneous formations

We first consider a hypothetical GCS repository consisting of a homogeneous storage formation and an AZMI formation, separated by a confining layer. Similar problem setups have been used previously in a number of analytical (Nordbotten et al., 2004) and numerical studies (Birkholzer et al., 2011; Class et al., 2009; Jung et al., 2013; Sun and Nicot, 2012) to simulate brine leakage into the AZMI. Fig. 1a shows a sketch of the problem set up. The domain has a single injection well and multiple potentially leaky wells. The forward model was solved following a semianalytical approach described in (Nordbotten et al., 2004, 2005b). We consider only brine leakage (i.e., before the actual $CO_2$ plume reaches the leaky wells). Fig. 1b shows typical temporal evolution of leakage rate (left axis) and the corresponding pressure buildup $\Delta p$ (right axis) for a single leaky site, using base case parameters listed in Table 1. For the particular curves shown in Fig. 1b, distances between the injection well and leaky site and between the leaky site and monitoring well are set to 100 and 200 m, respectively (note that the actual optimization problems presented below consider a large number of combinations of these distances). Both curves exhibit a sharp rise at early times before flattening. The detection threshold for pressure anomalies depends on a pressure gauge's accuracy and resolution. We set the $\Delta p$ detection threshold to 0.1 bar (1.45 psi), which may be obtainable using the current technology (K.R. Moelhoff, Schlumberger, written communication, March 7, 2013). Setting a higher detection threshold value would lead to longer first detection time and vice versa. Jung et al. (2013) also chose 0.1 bar as detection threshold, basing on natural variability considerations. Fig. 1b shows that the 0.1 bar detection threshold is reached in less than 10 days.

Results from two groups of tests will be presented below. In Group I, reservoir properties are assumed to be deterministic and only a single scenario is involved. The design objective is to determine the optimal number and locations of sensors while satisfying the BIPP constraints. Sensitivity studies are conducted to examine the effect of different parameters. The Group II tests expand

**Table 1**
Parameters used in base case.

| Parameter | Value |
|---|---|
| $CO_2$ density | 479 kg/m$^3$ |
| Brine density | 1045 kg/m$^3$ |
| $CO_2$ viscosity | $3.95 \times 10^{-5}$ Pa s |
| Brine viscosity | $2.54 \times 10^{-4}$ Pa s |
| Porosity[a] | 0.15 |
| Leaky-well permeability | $5 \times 10^{-12}$ m$^2$ |
| Well radius[b] | 0.15 m |
| $CO_2$ injection rate | 766 ton/d (1600 m$^3$/d) |
| Depth to top of AZMI | 1950 m |
| Storage formation thickness | 30 m |
| Confining layer thickness | 15 m |
| AZMI thickness | 30 m |
| AZMI permeability[a] | $2 \times 10^{-14}$ m$^2$ |
| Formation compressibility[a] | $6.4 \times 10^{-10}$ Pa$^{-1}$ |

[a] Same for both storage formation and AZMI.
[b] Same for both injection well and leaky well.

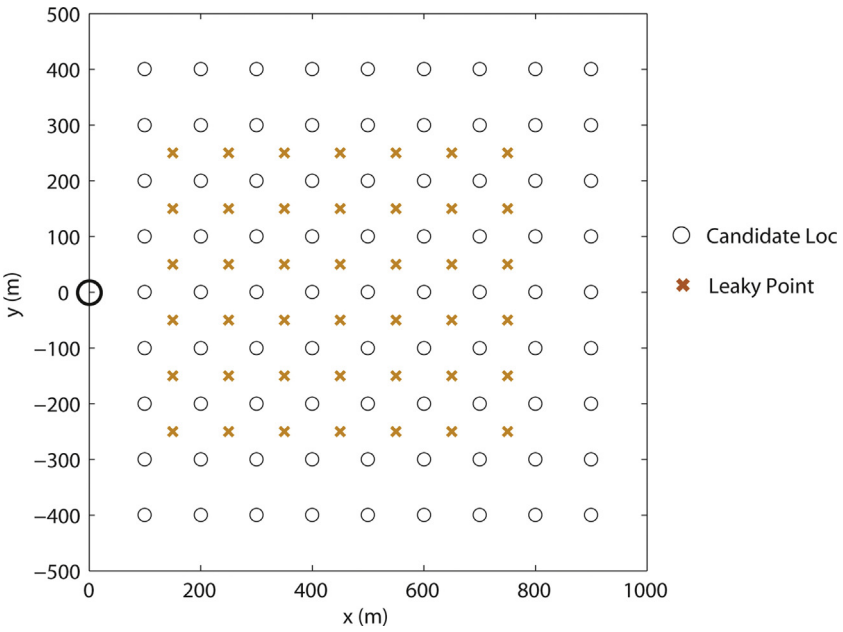


**Fig. 2.** Grids of leaky sites (×) and monitoring locations (O) used in Group I tests. Injection well is located at the origin (dark circle) but screened in the storage formation.

Group I by using multiple scenarios to account for parameter uncertainty. Unless otherwise specified, all model parameters used in this section are provided in Table 1.

### 3.1.1. Single scenario

Fig. 2 shows the plan view of AZMI, which has lateral dimensions of 1 km × 1 km. The injection well is located at the origin, but in the storage formation (not shown in figure). The potentially leaky sites are distributed uniformly across the inner domain, representing a situation in which little or no a priori knowledge on high-risk locations is available. The leaky site grid (× symbol) consists of $N_l = 42$ sites, which is to be covered by a 9 × 9 monitoring grid or, equivalently $N_m = 81$ potential monitoring sites (O symbol). The density of the monitoring grid is 100 m in both lateral directions. Our objective is to pick a subset of the monitoring grid to deploy a limited number of pressure gauges. Note that the actual outer boundary is assumed to be sufficiently far such that the semianalytical approach would be applicable. As mentioned before, all possible combinations of leaky sites and monitoring wells need to be considered in calculating the objective function and constraints in the BIPP. A leakage event is considered detected when $\Delta p$ observed at the monitoring well is greater than the detection threshold, at which time the accumulative leak volume is recorded and the monitoring well is added to subset $\mathcal{J}_d$. A single forward model run takes approximately 1.3 s to finish on a PC equipped with Intel core-i7 2.20 GHz CPU. Once the BIPP is formulated, the optimization problem itself can be solved within a couple of seconds using the Gurobi solver. The total number of decision variables is 3525 for the single-scenario case.

Fig. 3 plots two optimal network topologies (in the Pareto optimal sense) for $N = 3$ and $T_{max} = 25$ days. In Fig. 3a, the coverage ratio, defined as the fraction of leaky nodes covered out of all 42 potentially leaky sites, is 0.43, and the total volume of brine leaked during $T_{max}$ is 989 $m^3$. The specific design indicates that more than half of the leaky nodes will not be covered by any of the sensors if they leak. Combined coverage areas are provided in Fig. 3c to aid visualization of the results in Fig. 3a. To generate the coverage area of a sensor, we fixed the sensor location and varied leak locations systematically. Thus, each point on the contour shows the maximum $\Delta p$ a leak at that location can cause at the sensor location during $T_{max}$ (in this case, 25 days). The contours are made dimensionless by dividing actual $\Delta p$ by the detection threshold 0.1 bar. Because formation properties are homogeneous, the coverage contours manifest mainly the "distance" effect—leaky locations closer to the injection well lead to greater pressure buildups than those located further away. For each sensor, the pressure anomaly attenuates as the leaky point moves away from the sensor node. In this case, all three sensors were assigned to monitor potentially leaky sites that show greatest pressure increase, creating a significant overlap among the coverage regions of the three sensors. So could the location of the middle sensor be fixed and the other two sensors moved elsewhere to increase coverage? Fig. 3b and d show such a possibility, in which the sensors are more spread out and all leaky nodes are covered. The expected total leakage volume, however, also increases to 2670 $m^3$, which is almost three times greater than the case considered in Fig. 3a. Note that the particular sensor configuration in Fig. 3b is not symmetric around the center line as would be expected. This is because the optimization solver chose a slightly better objective function value. However, the asymmetry of network topology should not pose a concern in most practical situations; if desired, a symmetric solution that is only slightly worse than the Pareto optimal solution can be obtained (Meyer et al., 1994). In the current case, for example, symmetry is achievable by shifting the lower-right sensor node slightly so that it aligns vertically with the upper-right sensor node.

*3.1.1.1. Effect of number of sensors.* We systematically varied the upper bound of coverage, $B$, so that Pareto optimal sets (or Pareto front) were constructed for different objective function values. Fig. 4 shows the effect of number of sensors on Pareto optimal sets for $T_{max}$ fixed at 25 days. Increasing the number of sensors tends to reduce the leakage volume for the same coverage. On the other hand, increasing the number of sensors will increase the coverage if leakage volume is fixed. A site operator can inspect Fig. 4 to determine an appropriate tradeoff between monitoring costs and leakage. The turning point (or knee) of a Pareto front usually provides the optimal tradeoff between objectives. In the case of $N = 3$, for example, such a turning point solution exists around the coverage ratio equal to 0.72 and the total leakage volume of 1400 $m^3$. Fig. 4 also suggests that deploying more sensors may significantly boost the minimum coverage ratio (i.e., the lower-right point on the

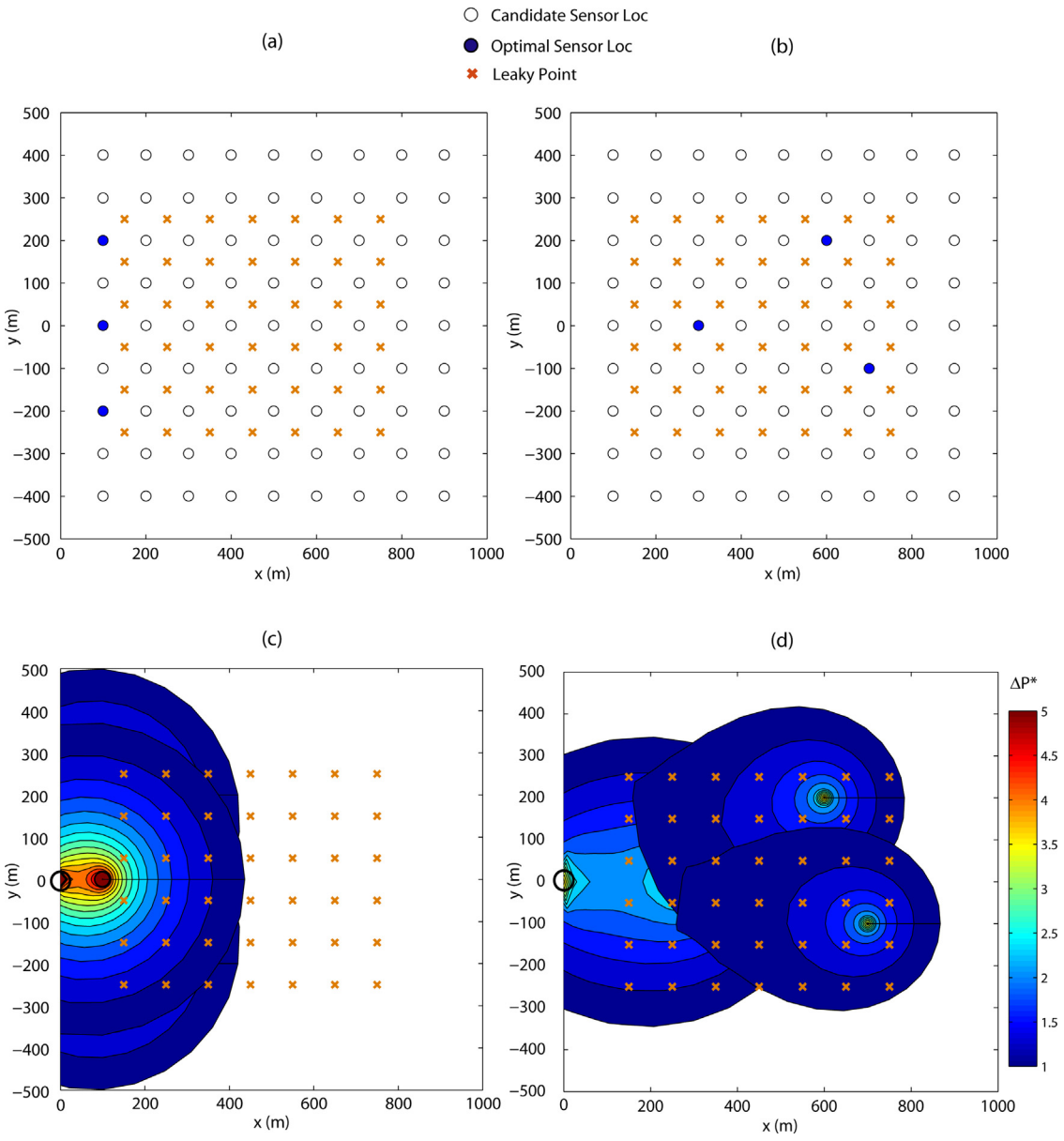


**Fig. 3.** Examples of Pareto optimal sensor configurations: (a) coverage ratio = 0.43; (b) coverage ratio = 1.0; (c) and (d) combined coverage areas corresponding to (a) and (b), respectively. Maximum detection time, $T_{max}$, is fixed at 25 days. Dimensionless contours in multiples of detection threshold (0.1 bar).

Pareto front), although it does not happen with the addition of every sensor. In this case, the change occurs only when the number of sensors is increased to five, after which the minimum coverage jumps to 0.71 from 0.43. This result is caused by the discrete design space, the particular spatial configuration of potentially leaky sites, and the shape of coverage area of each sensor. We will show a different example in Section 3.2.1.

*3.1.1.2. Effect of $T_{max}$.* Fig. 5 examines the effect of $T_{max}$ on Pareto sets. The total leakage volume is the smallest when $T_{max}$ is set to 10 days. However, the maximum coverage that can be achieved during $T_{max}$ = 10 days is less than 0.6 because the coverage area of each sensor is limited. Fig. 6 shows the maximum combined coverage of all three sensors for $T_{max}$ = 10 days. The corresponding total leakage volume is 1016 $m^3$. When $T_{max}$ is increased, the maximum coverage increases and so does the total leakage volume. At $T_{max}$ = 50 days, the Pareto set only includes two solutions, both have similar leakage volumes. Thus, this case highlights the significance of time dimension and the associated dilemma when designing pressured-based monitoring networks: tradeoffs between total leakage volumes and maximum coverage become relevant only when early detection is part of the objective and $T_{max}$ is made sufficiently tight; otherwise, the requirement on sensor locations can be significantly loosened.

*3.1.1.3. Effect of confining layer thickness.* Thickness of the confining layer inversely affects the magnitude of leakage flux if all other parameters are fixed. Fig. 7 shows the sensitivity of the Pareto optimal solutions to thickness of the confining layer for $N$ = 3 and $T_{max}$ = 25 days. A thicker confining layer (30 m) reduces leakage flux, as well as magnitudes of pressure anomalies. Therefore, the maximum coverage ratio is reduced compared to that of the base case, which uses a confining layer thickness of 15 m. On the other hand, a thinner confining layer (7.5 m) increases magnitudes of both leakage flux and pressure anomalies. The expected leakage volume is smaller and the coverage ratio is greater than that of the base case. This poses another dilemma related to GCS site selection: thicker

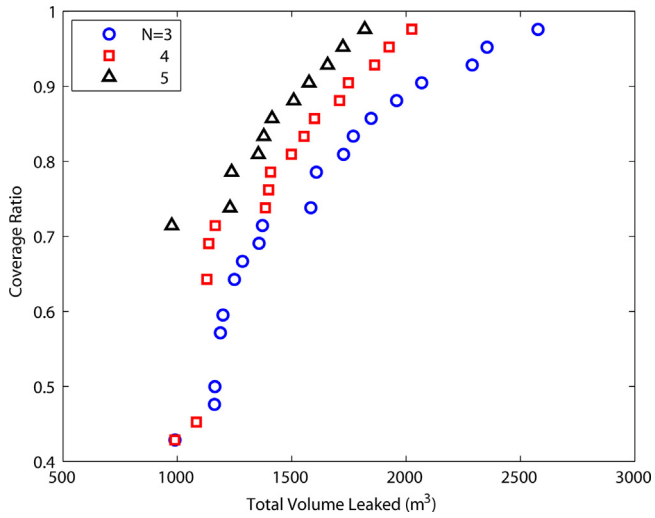


**Fig. 4.** Effect of number of sensors on Pareto optimal sets for $T_{max}$ = 25 days.

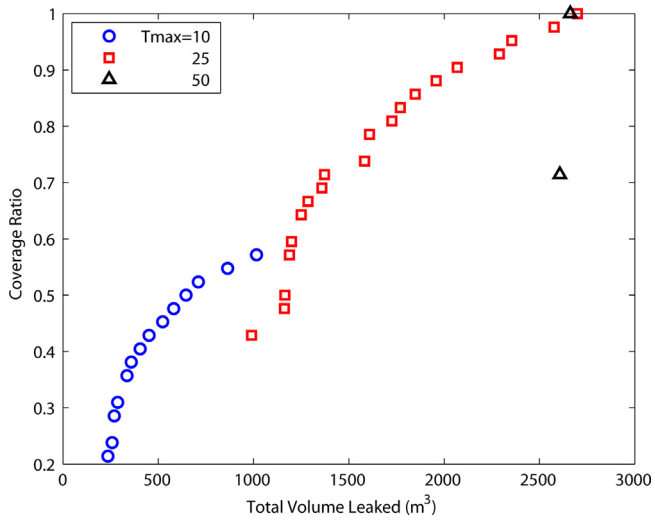


**Fig. 5.** Sensitivity of Pareto optimal sets to $T_{max}$ for $N$ = 3.

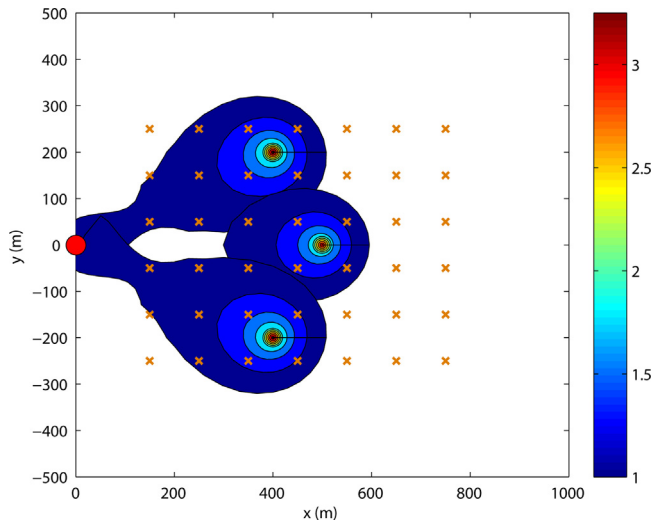


**Fig. 6.** Contour plot of maximum achievable coverage for $N$ = 3 and $T_{max}$ = 10 days.

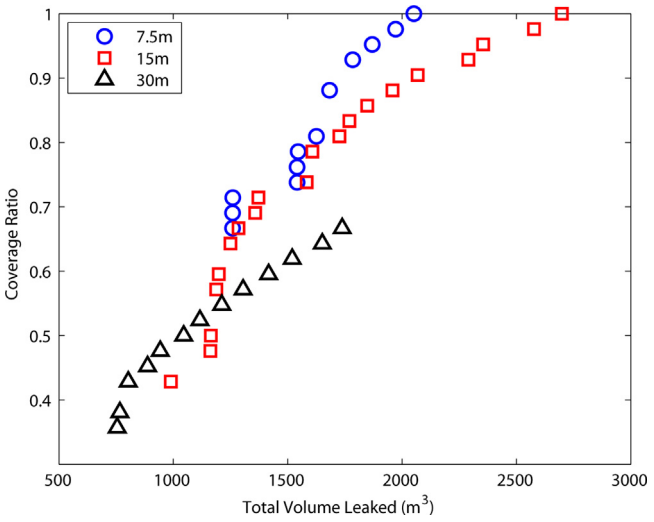


**Fig. 7.** Sensitivity of Pareto optimal sets to thickness of confining layer.

confining layer serves as a better natural barrier to leakage; however, it also reduces the likelihood of early detection in the AZMI.

### 3.1.2. *Multiple scenarios*

Multiple scenarios can be used to account for uncertainty in design parameters when the resulting number of design variables is still manageable. For demonstration, we assume that the storage formation permeability is uncertain. Its nominal value is equal to the base case value (i.e., $2 \times 10^{-14}$ m$^2$), and its lower and upper bounds are $9 \times 10^{-15}$ and $4 \times 10^{-14}$ m$^2$, respectively. First a sensitivity study was conducted by solving single-scenario BIPPs. Results show that the network design is relatively sensitive to permeability. The single-scenario Pareto sets for each of the three permeability values are plotted in Fig. 8. For $9 \times 10^{-15}$ m$^2$, the monitoring network is guaranteed to provide full coverage. For $4 \times 10^{-14}$ m$^2$, however, the maximum coverage is limited to be under 0.5. Avci (1994, Table 1) showed that pressure buildup is a function of the permeability ratio (denoted as $\alpha$ by Avci) between the AZMI and storage formation. Thus, instead of using absolute permeability values, one can use permeability ratios in sensitivity studies. For a given time, higher $\alpha$ value tends to result in greater leakage flux,

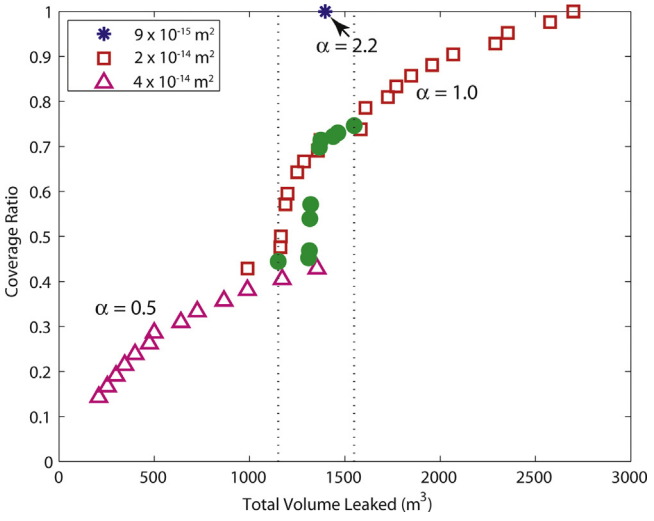


**Fig. 8.** Pareto optimal solutions obtained by solving a three-scenario problem (green circles bounded by dash lines). Single-scenario solutions corresponding to different permeability are also plotted. Permeability ratios ($\alpha$) labeled on the plot.

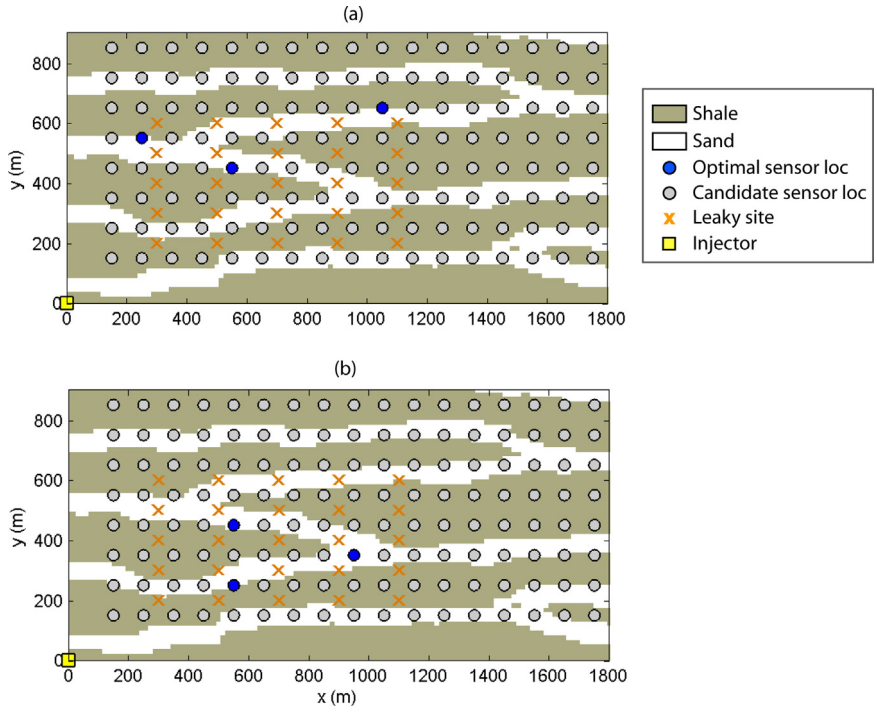


**Fig. 9.** Pareto optimal solutions corresponding to coverage ratio of (a) 0.3 and (b) 0.5 for binary-facies AZMI.

although the rate of increase diminishes when $\alpha$ approaches infinity. In the current case, the $\alpha$ values corresponding to the nominal, lower, and upper bound permeability are 1.0, 2.2, and 0.5, respectively. Thus, with all other parameters fixed, higher $\alpha$ improves detectability of the AZMI monitoring networks.

In the next step, a three-scenario BIPP was solved by considering the range of permeability values. The results are also plotted in Fig. 8 (filled circles). An immediate observation is that the range of three-scenario solutions is much narrower than that of the base case solution. This is because the three-scenario BIPP attempts to find a solution that is robust across all scenarios, at a price of slightly worse single-objective values. For the same coverage, the average total leaked volume given by the multi-scenario design is generally greater than that predicted by the single-scenario, base case design (i.e., most filled circles are to the right of square symbols in Fig. 8). Unlike the single-scenario base case in which perfect information is assumed to be available, the effect of parameter uncertainty in the three-scenario case is seen to make the Pareto front shift to the right (i.e., higher leaked volume). To reduce risks caused by the parameter uncertainty, one solution is to deploy more sensors, which will incur a higher monitoring cost.

### 3.2. Heterogeneous formations

In this section, we demonstrate the design of optimal monitoring networks for heterogeneous formations. Fig. 9a shows the problem setup. The domain size is 1800 m × 900 m, and the number of potential leaky sites is 25 (× symbol). Our goal is to select a subset of the monitoring grid (gray-color circle) to best monitor the leaky sites. The AZMI is assumed to have two dominant hydrofacies, which are referred to as *sand* and *shale* in the following discussion. The permeability values of sand and shale facies are set to $2 \times 10^{-14}$ and $1 \times 10^{-16}$ m$^2$, respectively. The multipoint statistical software, MPDS (Mariethoz et al., 2010), was used to generate facies distributions. MPDS is a pattern-based simulation program that uses training images to generate equally likely facies distributions, in which the training images serve as conceptualization of facies distributions in the field (Caers and Zhang, 2004). All other model parameters are similar to those used in the base case. In particular, the design detection time $T_{max}$ remains at 25 days. The forward model was solved numerically using the finite element software COMSOL (www.comsol.com), and all boundaries were assumed to be no-flow boundaries.

#### 3.2.1. Single scenario

In this first case, we assumed that the channel geometry is known exactly such that only a single scenario needs to be used. The example serves to illustrate the impact of preferential-flow channels on monitoring design. Fig. 9a and b show two Pareto optimal solutions obtained for coverage ratios of 0.3 and 0.5, respectively. In both solutions, all sensors are deployed exclusively in the

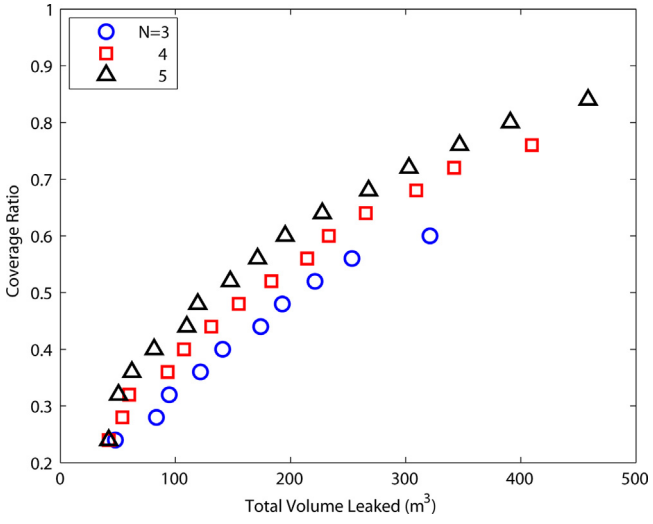


**Fig. 10.** Pareto sets obtained for different number of sensors for AZMI.

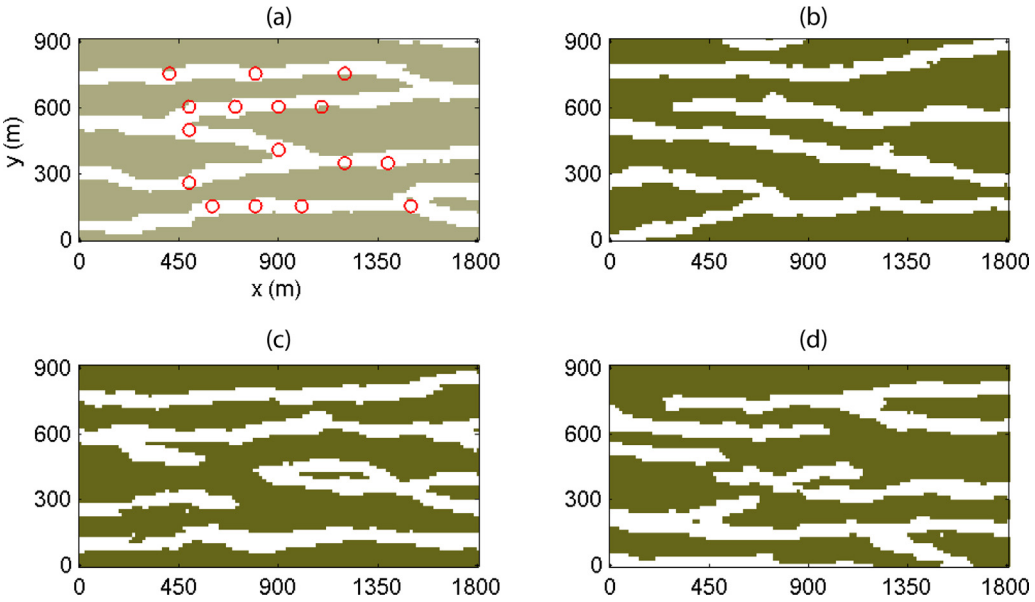


**Fig. 11.** (a) Locations of conditioning points (circles) overlain on reference field; (b), (c), and (d) examples of conditional facies realizations used in multi-scenario analysis.

higher-permeability sand facies. Deployed sensors in the former case are all clustered in one branch of the sand channel network that happens to have the large number of leaky sites. In the case of Fig. 9b, the sensors are more spread out to increase coverage, although at the price of higher expected total leakage. Fig. 10 plots Pareto optimal solutions for different number of sensors. The turning points of the Pareto fronts can be clearly identified on the plot. Compared with the similar case shown in Fig. 4 for the homogeneous aquifer problem, we note that the Pareto fronts obtained for the current case are smoother and no jump in coverage occurs as number of sensors increases. In addition, the lower bounds of all three curves are almost identical, although the upper bounds differ. This is because the leaky points intersecting the shale facies are essentially "shadowed" by those intersecting the sand channels and, thus, are essentially "blind" to the increase of sensors. Optimization revolves mainly around the subset of leaky points intersecting the sand channels. These observations highlight the need to identify large-scale heterogeneity during preliminary and continuous site characterization such that only the most risk significant locations are monitored. The total number of decision variables of the BIPP is 3561 in this case.

### 3.2.2. *Multiple scenarios*

In practice, facies distributions are inferred through limited borehole logs and other sources of "soft" information such as seismic survey data, resulting in significant uncertainty in locations

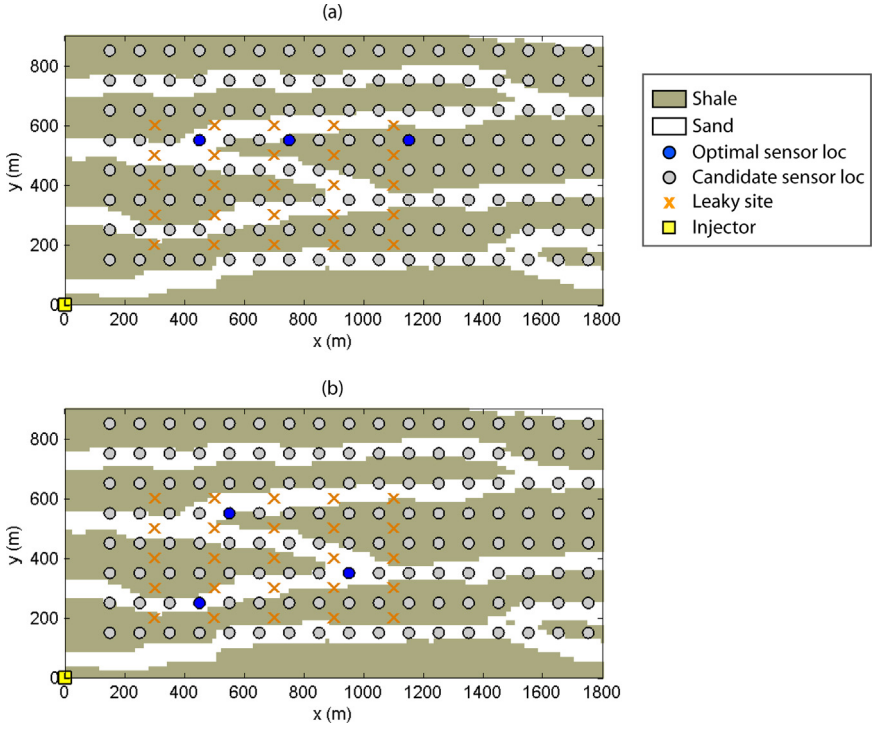


**Fig. 12.** Optimal sensor locations identified under facies-distribution uncertainty for coverage ratios of (a) 0.3 and (b) 0.5, respectively based on the 20-scenario run.

without measurements. Multiple scenarios may be constructed to incorporate the effect of uncertain facies distributions. To demonstrate such a case, we assume that facies types are available at only a number of borehole locations (open circles in Fig. 11a) and most of the data show sand facies, as can be seen in Fig. 11a. Conditional realizations of facies distributions are created, which all honor the same conditioning data but exhibit distinctively different spatial structures in locations away from the conditioning points. Fig. 11b–d show three examples of such conditional facies realizations. We treat each conditional realization as a scenario. The uncertainty is reflected in both the geometry and connectivity of simulated sand channels. Assuming that all scenarios have equal likelihoods, our goal is to find the expected optimal monitoring locations by averaging across all scenarios. We tested 10, 20, and 30 scenarios (realizations) and the resulting BIPP decision variables were 34,386, 68,636, and 102,886, respectively. We found that optimal sensor locations identified by the 20- and 30-scenario runs are close to each other, and both differ from those of the 10-scenario run. Therefore, we use results from the 20-scenario run for faster solution speed.

Fig. 12 shows the optimal sensor locations identified for two different coverage ratios, 0.3 and 0.5, respectively, based on the 20-scenario run. For the case of 0.3 (Fig. 12a), two of the three sensors are placed near the edge of shale facies, although they remain close to the largest cluster of potentially leaky points in sand channel facies; the average expected leakage is 115 $m^3$. For a coverage ratio of 0.5, Fig. 12b shows that the optimal sensor locations are more spread out, but similar to those obtained in the case with perfect information (i.e., Fig. 9b); the average expected leakage is 270 $m^3$. The effect of facies distribution uncertainty is manifested in less optimal monitoring locations than those obtained in the perfect-information case and higher expected leakage.

We see in this example that as the number of scenario increases, the number of decision variables grows quickly. Therefore, for cases involving many equally likely scenarios a better approach is to identify bounding scenarios, if possible, and then perform optimization.

## 4. Summary and conclusions

Deep subsurface, pressure-based monitoring is a key MMV technology for many GCS sites because of its early detection capability. Optimization of monitoring network designs not only reduces risks, but also saves long-term operational costs of GCS sites. In this work, we formulated a BIPP for optimizing sensor placements under fixed budgets while maximizing coverage and minimizing total leakage caused by focused leakage pathways. The leakage volume is used as a proxy for environmental damage. This work mainly considered brine leakage into AZMI, which may affect larger areas (due to pressurization) than $CO_2$ plume does and its adverse effect on drinking water aquifers has been largely overlooked in previous studies. Nevertheless, our technical approach is general and allows for consideration of both conceptual and model parameter uncertainty. An important notion introduced through this work is the maximum detection time, $T_{max}$, which has both practical and regulatory significance. Only when $T_{max}$ is clearly defined and incorporated into a site-specific risk management plan can the optimization problem exist. Design using BIPP was demonstrated for both homogeneous and heterogeneous formations. In each case, we showed how to generate Pareto optimal sets for site operators to make tradeoffs between the two monitoring objectives.

For homogeneous formations, our sensitivity analyses clearly show the effects of sensor quantity, duration of $T_{max}$, confining layer thickness, and permeability ratio on the optimal monitoring network design. Increasing the number of sensors will reduce both leakage volume and uncovered sites. Increasing $T_{max}$ can improve coverage, but also significantly increase the expected total leakage. A thicker confining layer tends to reduce the maximal coverage that can be attained, although total leakage volume is also decreased because of reduced leakage flux. Finally, the network design is sensitive to the transmissivity ratio $\alpha$ because higher $\alpha$ leads to increased flux. For heterogeneous formations, our results reveal the value of information to monitoring design. Incomplete or inaccurate site characterization can adversely affect the chance of intercepting anomalies, especially in the presence of continuous preferential flow channels.

Although only hypothetical examples are given, the BIPP presented in this work is general and can be applied to a wide range of GCS sites. In practice, we envision a three-stage design process:

- In the first stage, the monitoring locations (i.e., the set $\mathcal{I}$) are identified and, if possible, prioritized based on site characterization information. A global sensitivity study may be conducted at this stage to identify the most influential parameters to the monitoring objectives, basing on which scenarios (i.e., the set $\mathcal{S}$) can be created to incorporate parameter uncertainty.
- In the second stage, a damage function needs to be defined according to regulatory policies and site-specific risk criteria. Although many viewed the definition of a damage function as an insurmountable task because of the lack of reported incidents, others suggested focusing on the consequence rather than probability of failure such that a cost-benefit-risk analysis can be performed and financial liabilities be evaluated (Price and Oldenburg, 2009; Trabucchi et al., 2010). Even in the absence of a clearly defined damage function, one can still perform monitoring design using a proxy measure such as the total volume of leakage used in this study.
- The remaining task of the design is to solve the BIPP and compare different design options. The combinatorial problem requires running the forward model many times to optimize the monitoring site locations. Instead of the full-scale model we used, a reduced-order or metamodel may be trained and then applied to speed up the optimization process.

Application of the aforementioned three-stage process is likely to be iterative and may be concurrent with continuous site characterization activities.

## Acknowledgments

We thank the associate editor and two anonymous reviewers for their constructive comments. A. Sun and J.-P. Nicot are partly funded by EPA STAR Grant R834384. Publication authorized by the Director, Bureau of Economic Geology.

## References

Avci, C.B., 1994. Evaluation of flow leakage through abandoned wells and boreholes. Water Resour. Res. 30, 2565–2578.

Bayer, P., de Paly, M., Bürger, C.M., 2010. Optimization of high-reliability-based hydrological design problems by robust automatic sampling of critical model realizations. Water Resour. Res. 46, W05504.

Benson, S.M., 2007. Monitoring GS of carbon dioxide. In: Wilson, E.J., Gerard, D. (Eds.), Carbon Capture and GS: Integrating Technology, Monitoring and Regulation. Blackwell Scientific Publishing, Ames, IA.

Berry, J., Hart, W.E., Phillips, C.A., Uber, J.G., Watson, J.P., 2006. Sensor placement in municipal water networks with temporal integer programming models. J. Water Resour. Plan. Manag. 132, 218–224.

Birkholzer, J.T., Nicot, J.P., Oldenburg, C.M., Zhou, Q., Kraemer, S., Bandilla, K., 2011. Brine flow up a well caused by pressure perturbation from geologic carbon sequestration: static and dynamic evaluations. Int. J. Greenh. Gas Con. 5, 850–861.

Birkholzer, J.T., Zhou, Q., 2009. Basin-scale hydrogeologic impacts of $CO_2$ storage: capacity and regulatory implications. Int. J. Greenh. Gas Con. 3, 745–756.

Boyd, S., Vandenberghe, L., 2004. Convex Optimization. Cambridge University Press.

Buscheck, T., Friedmann, S., Sun, Y., Chen, M., Hao, Y., Wolery, T., Aines, R., 2012. Active $CO_2$ reservoir management for $CO_2$ capture, utilization, and storage: an approach to improve $CO_2$ storage capacity and to reduce risk. In: Carbon Management Technology Conference.

Caers, J., Zhang, T., 2004. Multiple-point geostatistics: a quantitative vehicle for integrating geologic analogs into multiple reservoir models. AAPG Mem., 383–394.

Celia, M.A., Nordbotten, J.M., Court, B., Dobossy, M., Bachu, S., 2011. Field-scale application of a semi-analytical model for estimation of $CO_2$ and brine leakage along old wells. Int. J. Greenh. Gas Con. 5, 257–269.

Cihan, A., Zhou, Q., Birkholzer, J.T., 2011. Analytical solutions for pressure perturbation and fluid leakage through aquitards and wells in multilayered-aquifer systems. Water Resour. Res. 47, W10504.

Class, H., Ebigbo, A., Helmig, R., Dahle, H., Nordbotten, J., Celia, M., Audigane, P., Darcis, M., Ennis-King, J., Fan, Y., Flemisch, B., Gasda, S., Jin, M., Krug, S., Labregere, D., Naderi Beni, A., Pawar, R., Sbai, A., Thomas, S., Trenty, L., Wei, L., 2009. A benchmark study on problems related to $CO_2$ storage in geologic formations. Comput. Geosci. 13, 409–434.

Dhar, A., Datta, B., 2007. Multiobjective design of dynamic monitoring networks for detection of groundwater pollution. J. Water Resour. Plan. Manag. 133, 329–338.

DOE/NETL, 2011. Best Management Practices for Risk Analysis and Simulation for Geologic Storage of $CO_2$. National Energy Technology Laboratory, Pittsburgh, PA.

Dooley, J.J., Trabucchi, C., Patton, L., 2010. Design considerations for financing a national trust to advance the deployment of geologic $CO_2$ storage and motivate best practices. Int. J. Greenh. Gas Con. 4, 381–387.

Gurobi, 2012. Gurobi Optimization Solver. http://www.gurobi.com/

Hovorka, S.D., Meckel, T.A., Treviño, R.H., 2013. Monitoring a large-volume injection at Cranfield, Mississippi—project design and recommendations. Int. J. Greenh. Gas Con..

Jung, Y., Zhou, Q., Birkholzer, J.T., 2013. Early detection of brine and $CO_2$ leakage through abandoned wells using pressure and surface-deformation monitoring data: concept and demonstration. Adv. Water Resour..

Krause, A., Leskovec, J., Guestrin, C., VanBriesen, J., Faloutsos, C., 2008. Efficient sensor placement optimization for securing large water distribution networks. J. Water Resour. Plan. Manag. 134, 516–526.

Lewicki, J.L., Hilley, G.E., Oldenburg, C.M., 2005. An improved strategy to detect $CO_2$ leakage for verification of geologic carbon sequestration. Geophys. Res. Lett. 32, L19403.

Loaiciga, H.A., 1989. An optimization approach for groundwater quality monitoring network design. Water Resour. Res. 25, 1771–1782.

Loaiciga, H.A., Charbeneau, R.J., Everett, L.G., Fogg, G.E., Hobbs, B.F., Rouhani, S., 1992. Review of ground-water quality monitoring network design. J. Hydraul. Eng. 118, 11–37.

Lunt, I., Bridge, J., Tye, R., 2004. A quantitative, three-dimensional depositional model of gravelly braided rivers. Sedimentology 51, 377–414.

Mahar, P.S., Datta, B., 1997. Optimal monitoring network and ground-water-pollution source identification. J. Water Resour. Plan. Manag. 123, 199–207.

Mariethoz, G., Renard, P., Straubhaar, J., 2010. The Direct Sampling method to perform multiple-point geostatistical simulations. Water Resour. Res. 46.

Meyer, P.D., Valocchi, A.J., Eheart, J.W., 1994. Monitoring network design to provide initial detection of groundwater contamination. Water Resour. Res. 30, 2647–2659.

Nordbotten, J.M., Celia, M.A., Bachu, S., 2004. Analytical solutions for leakage rates through abandoned wells. Water Resour. Res. 40.

Nordbotten, J.M., Celia, M.A., Bachu, S., 2005a. Injection and storage of $CO_2$ in deep saline aquifers: analytical solution for $CO_2$ plume evolution during injection. Transport Porous Med. 58, 339–360.

Nordbotten, J.M., Celia, M.A., Bachu, S., Dahle, H.K., 2005b. Semianalytical solution for $CO_2$ leakage through an abandoned well. Environ. Sci. Technol. 39, 602–611.

Nuñez-López, V., Hovorka, S.D., Wolaver, B.D., Zahid, K.M., Sun, A.Y., Hosseini, S.A., Romanak, K.D., 2011. Monitoring verification and accounting (MVA) for the Lake Charles CCS Project. Final report prepared for Denbury Onshore, LLC, under DOE Award Number: DE-FE-0002314. Bureau of Economic Geology, The University of Texas at Austin, pp. 126.

Oladyshkin, S., Class, H., Helmig, R., Nowak, W., 2011. An integrative approach to robust design and probabilistic risk assessment for $CO_2$ storage in geological formations. Comput. Geosci. 15, 565–577.

Oldenburg, C.M., Unger, A.J.A., 2003. On leakage and seepage from geologic carbon sequestration sites unsaturated zone attenuation. Vadose Zone J. 2, 287–296.

Price, P.N., Oldenburg, C.M., 2009. The consequences of failure should be considered in siting geologic carbon sequestration projects. Int. J. Greenh. Gas Con. 3, 658–663.

Pruess, K., 2004. Numerical simulation of $CO_2$ leakage from a geologic disposal reservoir, including transitions from super- to subcritical conditions, and boiling of liquid $CO_2$. SPE J. 9, 237–248.

Reed, P.M., Minsker, B.S., 2004. Striking the balance: long-term groundwater monitoring design for conflicting objectives. J. Water Resour. Plan. Manag. 130, 140–149.

Romanak, K., Bennett, P., Yang, C., Hovorka, S.D., 2012. Process-based approach to $CO_2$ leakage detection by vadose zone gas monitoring at geologic $CO_2$ storage sites. Geophys. Res. Lett. 39, L15405.

Rutqvist, J., Vasco, D.W., Myer, L., 2010. Coupled reservoir-geomechanical analysis of $CO_2$ injection and ground deformations at In Salah, Algeria. Int. J. Greenh. Gas Con. 4, 225–230.

Seto, C.J., McRae, G.J., 2011. Reducing risk in basin-scale $CO_2$ sequestration: a framework for integrated monitoring design. Environ. Sci. Technol. 45, 845–859.

Singh, A., Minsker, B.S., 2008. Uncertainty-based multiobjective optimization of groundwater remediation design. Water Resour. Res. 44, W02404.

Stadler, W., 1988. Multicriteria Optimization in Engineering and in the Sciences. Springer.

Stenhouse, M.J., Gale, J., Zhou, W., 2009. Current status of risk assessment and regulatory frameworks for geological $CO_2$ storage. Energy Procedia 1, 2455–2462.

Sun, A.Y., Nicot, J.P., 2012. Inversion of pressure anomaly data for detecting leakage at geologic carbon sequestration sites. Adv. Water Resour., 20–29.

Sun, A.Y., Painter, S.L., Wittmeyer, G.W., 2006. A robust approach for iterative contaminant source location and release history recovery. J. Contam. Hydrol. 88, 181–196.

Sun, A.Y., Ritzi, R.W., Sims, D.W., 2008. Characterization and modeling of spatial variability in a complex alluvial aquifer: implications on solute transport. Water Resour. Res. 44, W04402, http://dx.doi.org/10.1029/02007WR006119.

Sun, A.Y., Zeidouni, M., Nicot, J.P., Lu, Z., Zhang, D., 2013. Assessing leakage detectability at geologic $CO_2$ sequestration sites using the probabilistic collocation method. Adv. Water Resour., 49–60.

Trabucchi, C., Donlan, M., Wade, S., 2010. A multi-disciplinary framework to monetize financial consequences arising from CCS projects and motivate effective financial responsibility. Int. J. Greenh. Gas Con. 4, 388–395.

U.S. Energy Information Administration, 2012. http://www.eia.gov/todayinenergy/detail.cfm?id=7290 (accessed 15.01.13).

U.S. Environmental Protection Agency, 2010. Geologic $CO_2$ Sequestration Technology and Cost Analysis. EPA, Washington, DC.

Uciński, D., Patan, M., 2007. D-optimal design of a monitoring network for parameter estimation of distributed systems. J. Global Optimiz. 39, 291–322.

Wilson, E.J., Friedmann, S.J., Pollak, M.F., 2007. Research for deployment: incorporating risk, regulation, and liability for carbon capture and sequestration. Environ. Sci. Technol. 41, 5945–5952.

Wilson, E.J., Morgan, M.G., Apt, J., Bonner, M., Bunting, C., Gode, J., Haszeldine, R.S., Jaeger, C.C., Keith, D.W., McCoy, S.T., Pollak, M.F., Reiner, D.M., Rubin, E.S., Torvanger, A., Ulardic, C., Vajjhala, S.P., Victor, D.G., Wright, I.W., 2008. Regulating the geological sequestration of $CO_2$. Environ. Sci. Technol. 42, 2718–2722.

Xu, J., Johnson, M.P., Fischbeck, P.S., Small, M.J., VanBriesen, J.M., 2010. Robust placement of sensors in dynamic water distribution systems. Eur. J. Oper. Res. 202, 707–716.

Yang, Y.M., Small, M.J., Ogretim, E.O., Gray, D.D., Bromhal, G.S., Strazisar, B.R., Wells, A.W., 2011. Probabilistic design of a near-surface $CO_2$ leak detection system. Environ. Sci. Technol. 45, 6380–6387.

Young, S.C., Kelley, V., Budge, T., Deeds, N.E., Ewing, T.E., 2006. Development of a detailed groundwater model for the Chicot and Evangeline aquifers in Colorado, Wharton, and Matagorda Counties, Texas. URS Corporation and Intera Inc., pp. 118.

Zhou, Q., Birkholzer, J.T., Tsang, C.-F., Rutqvist, J., 2008. A method for quick assessment of $CO_2$ storage capacity in closed and semi-closed saline formations. Int. J. Greenh. Gas Con. 2, 626–639.

Zou, Y., Chakrabarty, K., 2004. Uncertainty-aware and coverage-oriented deployment for sensor networks. J. Parallel Distribut. Comput. 64, 788–798.